Supporting Information

Flexible plasmonic modulators induced by the thermomechanical effect

Qiushun Zou[‡ab], Wenjie Liu[‡a], Yang Shen*[a], Chongjun Jin*[a]

[a] State Key Laboratory of Optoelectronic Materials and Technologies, School of Materials Science and Engineering, Sun Yat-sen University, Guangzhou 510275, China

[b] School of Electronics and Information Technology, Sun Yat-sen University, Guangzhou 510275, China

‡ Contributed equally to this work

* E-mail: jinchjun@mail.sysu.edu.cn, sheny@mail2.sysu.edu.cn

S1. The fabrication procedure of the MSWA on the PDMS

The nanofabrication procedure is schematically shown in Fig. 2a. A silver film of 150 nm was first deposited on the (100) p-doped silicon wafer by electron-beam evaporation (Wavetest, DE400). The deposition rate and base pressures were 0.8 Å/s and 5×10^{-7} mbar, respectively. A film of poly (methyl methacrylate) (PMMA) was then spin-coated at 6000 rpm for 1 min and baked for 3.5 min at 173 °C. Its thickness was ~470 nm. The PMMA film was thereafter subjected to a standard electron beam lithography (EBL, Riath, EBPG5000+) and subsequent developing to form the complementary structure of MSWA in advance. Then a 30 nm layer of gold was deposited on the pattern array with the deposition rate of 1Å/S and a base pressure of 5×10^{-7} mbar by electron-beam evaporation. The gold MSWA on silver/silicon support was finally obtained through a standard lift-off process.

To prepare PDMS substrates, a liquid-state mixture of the base and the curing agent (Sylgard 184, Dow Corning) at a ratio of 10:1 in weight was poured into the petri dish with a piece of 4-inch silicon, degassed in a vacuum desiccator for approximately 30 min, and cured at 70 °C for 2 h to generate a flat PDMS slab. To avoid undesired buckling and cracking of the MSWA due to the deformation of PDMS during the transfer process, the PDMS slab was immobilized on the glass in advance. After that, the Ag-film-supported MSWA was brought into tightly contacting with the flat surface of PDMS slab for 12 hours. Followed by peeling off the silicon wafer, and the

MSWA /Ag film structure was transferred to the flexible PDMS slab due to the stronger adhesive between the PDMS and silver film than that between the silver and silicon. Finally, the silver film was removed by phosphorous acid, giving rise to the resultant MSWA on the PDMS. The SEM image of a unit cell of the "meander near the straight wire" structure on the silver film is shown in Fig. S1. The gap width between the meander and straight wire is 55 nm.

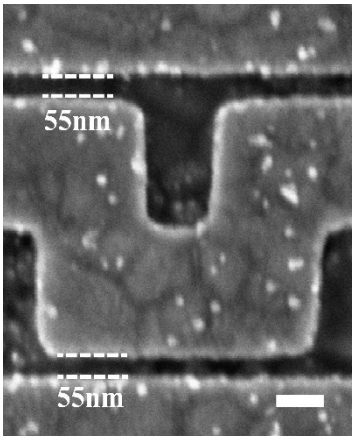

Fig. S1. SEM image of a unit cell of the "meander near the straight wire" structure on the silver film, where the gap width is 55 nm. Scale bar: 100 nm

S2. Experimental Setup

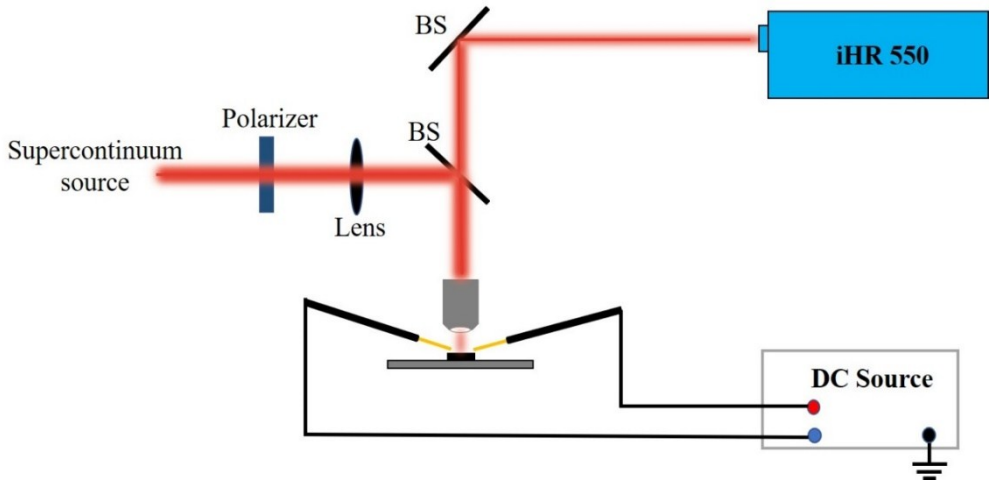

Fig. S2. Schematic of the experimental setup.

The setup for the reflectance spectra measurement is schematically in Fig. S2. A white-light supercontinuum source (NKT, Photonics) was polarized by a Glan-Taylor prism and collimated by a lens and 50× objective (Olympus LMPlan IR, NA 0.55) to generate a quasi-parallel light with the beam spot of 12 μm in diameter. This beam was illuminated on the sample. The reflected light was collected by the same objective and finally coupled to a spectrometer (iHR550, Horiba). The

spectra were corrected by the reflection spectrum of a standard silver mirror. The current was injected by two probes connected with a DC Source Meter (M8831, Maynuo).

S3. Measured reflection spectra of MSWA when the polarization of the incident light is perpendicular to the stripes.

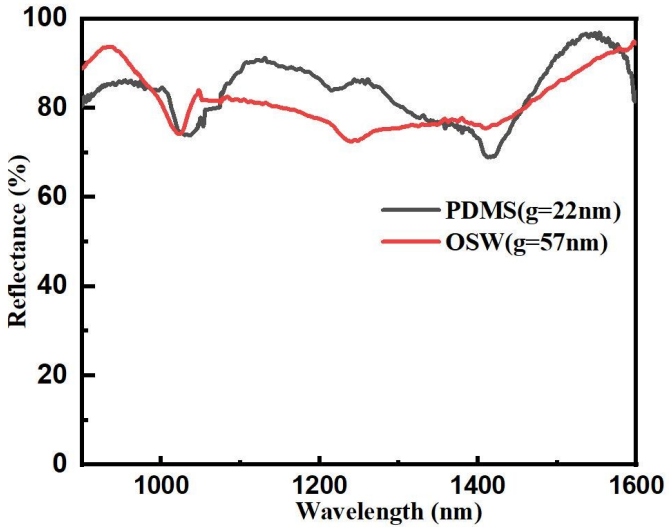

Fig. S3. Measured reflection spectra of MSWAs on PDMS and OSW substrates when the polarization of the incident light is perpendicular to the gold wires.

S4. The MSWA on the oxidized silicon wafer

The MSWA on an oxidized silicon wafer (OSW) with a layer of 500 nm silicon dioxide was manufactured by the standard electron beam lithography procedure. The PMMA film with a thickness of 470 nm was first spin-coated on the surface of the oxidized silicon wafer, and subsequently baked at 173°C for 3.5 min. The complementary structure of MSWA was then patterned thought the EBL and subsequent developing. After electron-beam evaporation of 30-nm gold and lift-off process, the MSWA on OSW was finally obtained. The SEM image of the MSWA on the OSW is shown in Fig. S4a.

We simulated the reflectance spectrum of the MSWA on the OSW through the FDTD method. The reflectance spectrum exhibits a resonant dip at a wavelength of 1059 nm (the red solid curve, the position is marked by D' in Fig. S4b). To further identify the origin of this resonance, we also plotted the normalized electric field intensity distributions at this wavelength as shown in Fig. S4c-d. The concentration of electric field in the gap between the meander and straight wires indicates that the resonance mode is caused by the excitation of localized surface

plasmon resonances (LSPRs), which is similar to the resonant mode D for the MSWA on the PDMS substrate. We also measured the reflectance spectra of the MSWA on the OSW as the injected current continuously increases from 0 to 60 mA, as shown in Fig. S4e. It is found that there is no observable change in reflectance with the increasing current injection. This result reveals that the effect of the carrier injection and electromigration can be neglected in our experiments. In addition, The linear volt-ampere characteristic indicates that the resistance of the MSWA on the OSW is invariable as the current injection is increased from 0 to 60 mA (Fig. S4f).

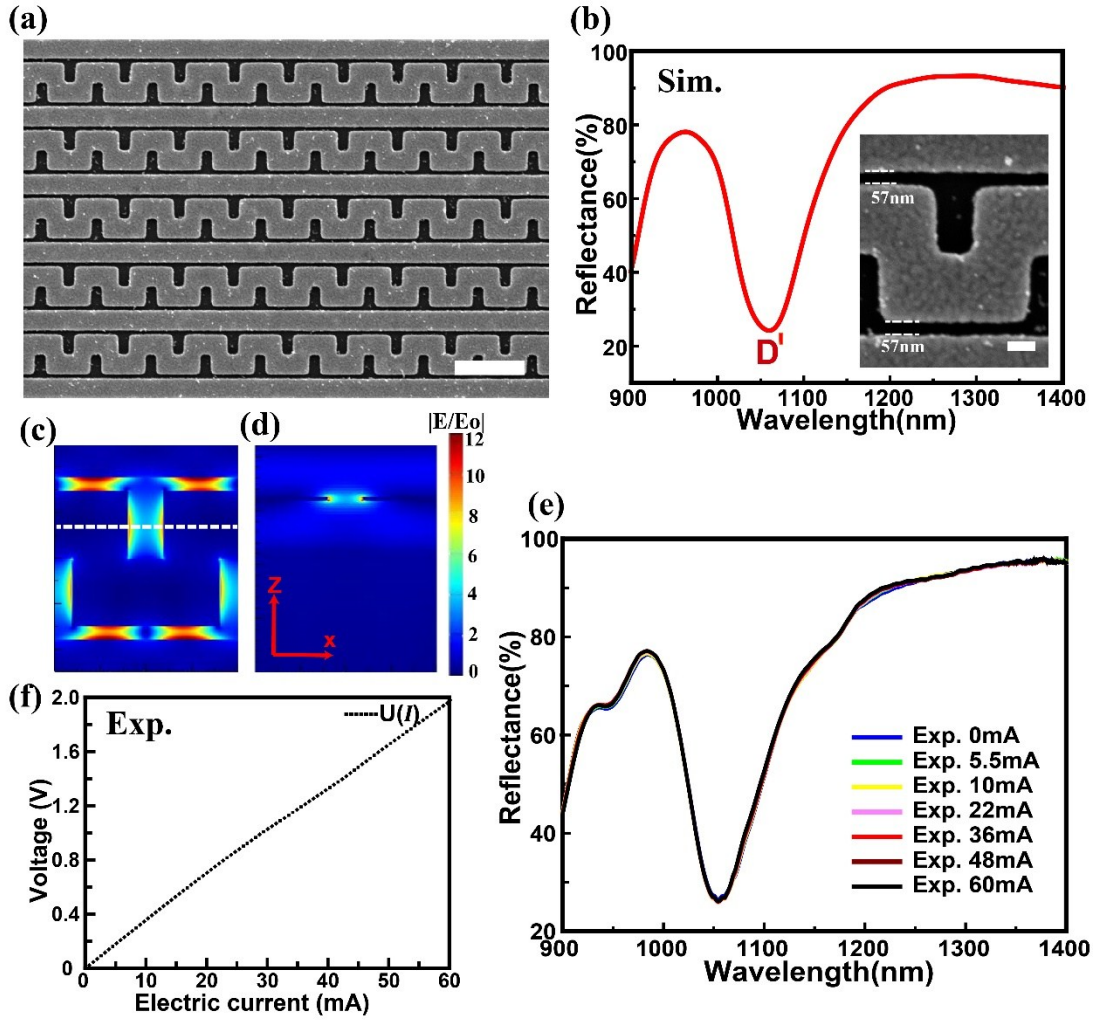

Fig. S4. (a) Top-view SEM image: the MSWA on the OSW with 500 nm-thickness silicon dioxide. (b) Simulated reflectance spectrum when the polarization of the incident wave is parallel to the gold wire. Inset is a unit cell of the MSWA on the OSW, and the gap width between the meander and straight wire is 57 nm. The dip is marked by D' at λ=1059 nm. (c) The electric field intensity distribution at the plane of z =15 nm (where the top-surface of the OSW is z=0 nm) at the dip D'. (e) The electric field intensity distribution at the x-z cross section (marked by a dashed line in (c)) at the at the dip D'. (e) The measured reflectance spectra as the injected currents varied from 0 to 60 mA. (f) Volt-ampere characteristics. Scale bar: (a) 1 μm and inset of (b) 100 nm.

S5. Charge density distribution of the MSWA on PDMS substrate after current injection.

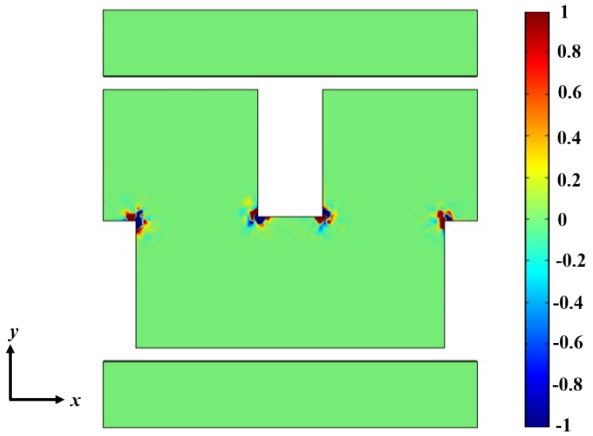

Fig. S5. Normalized charge density distribution of the MSWA on PDMS substrate after current injection.

S6. The optical and thermomechanical co-simulations

The optical simulations were performed using commercial software (FDTD solutions, Lumerical) to generate the reflectance spectra and electric field intensity distributions. Plane-waves with the polarization parallel to the straight wire (*x*-direction) were used to excite the structures. The Bloch boundary conditions were applied in both *x*- and *y*-direction. A mesh size of 1 nm for the metal region was utilized. The dielectric permittivity of gold is taken from the tabulated data.[1] The used refractive indices of PDMS was 1.45.[2]

To verify the effect of the local Joule heating, we construct a 3D model to investigate the thermomechanical deformation of the PDMS by the finite method (FEM). In the thermomechanical frame, we modeled this system as only a PDMS slab with a thickness of 1 mm to evaluate this deformation. For simplicity, the entire PDMS slab was divided into two parts: the heated region and the surrounding region (see Fig. S6a), which correspond to the area covered with and without the MSWA, respectively. The areas of the heated region and entire surface were set to 37×23 μm^2 (45*P_x×25*P_y) and 66×55 μm^2, respectively. The antiperiodic boundary conditions were applied for the outmost boundary of the surrounding region along *x*- and *y*-direction, respectively. The fixed constraint was utilized at the bottom of the PDMS. A series of temperatures *T* (correspond to the temperature of the real experiment) were loaded on the entire top-surface of the heated region. The applied Young's modulus and Poisson ratios for the PDMS

were 2 Mpa and 0.49, respectively.[3] The thermal expansion coefficient of PDMS and gold were $(9\times10^{-4}/K)$[4] and $(14.4\times10^{-6}/K)$[5], respectively. The conduct thermal coefficient between the heated region and the surrounding region was 0.16W/(m*K).[4]

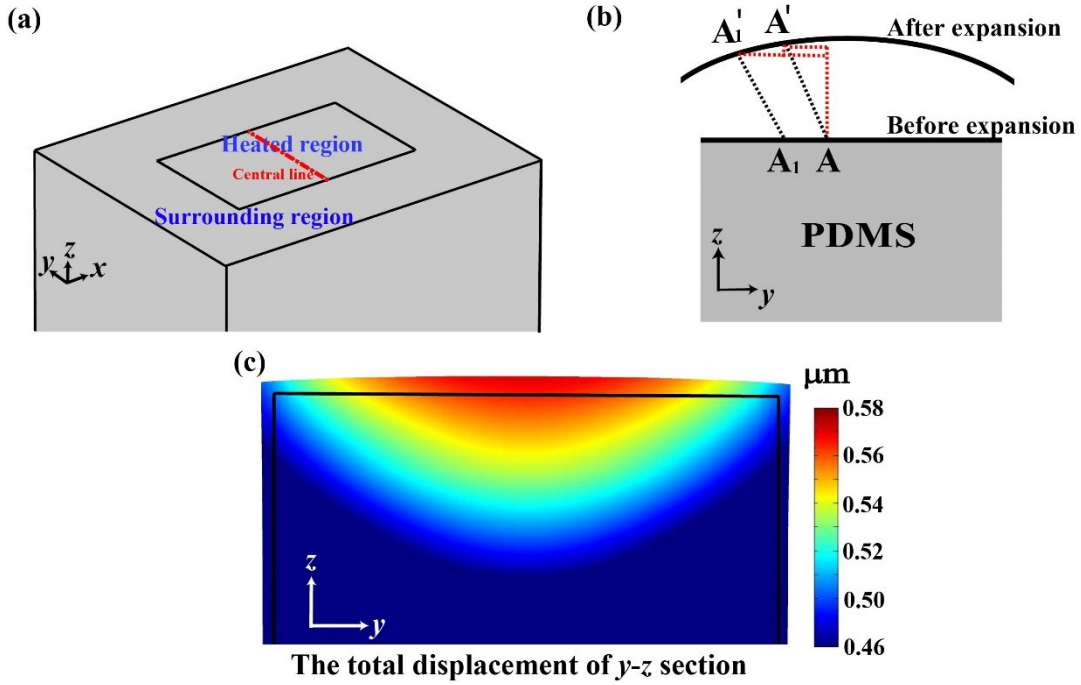

Fig. S6. (a) The heated and the surrounding regions. The red dashed line represents the central line of the heated region. (b) Geometry of the *y*-*z* cross-section along the central line of the heated region. (c) The total displacement *u* distribution of the central *y*-*z* cross-section of the heated region with an applied temperature of 312.91 K.

The simulated results demonstrate that the center PDMS was driven to arch upward as the PDMS of the heated region was heated by the local Joule heat. This bump will lead to the widening of the gap distance between the meander and straight wire. The displacement u_x of *x*-direction is restricted to the high-stiffness of bulk gold strips within a sustainable range of thermo-deformation. Therefore, the resonance response of the MSWA on the PDMS is mainly codetermined by the displacements u_y and u_z along the *y*- and *z*-directions, respectively. To examine the uniformity of the gap width changes in response to the elevated temperatures, we calculated the gap width between the meander and straight wire at the different area but along the central line (see Fig. S6a). The geometry of the central *y*-*z* section is plotted in Fig. S6b. We assume that, due to the thermal deformation, the initial positions A_1 and A with an original interval of P_y (0.909 μm, namely the border of a unit cell) moves to the positions A_1' and A',

respectively. The u_{yA}, u_{zA} and u_{yA_1}, u_{zA_1} represent the displacement of the positions A and A_1 along the *y*- and *z*-directions, respectively. Thus, the gap distance between the meander and straight wire can be calculated by the following equation:

$$g = \frac{\sqrt{\left(AA_1 + u_{yA_1} - u_{yA}\right)^2 + \left(u_{zA} - u_{zA_1}\right)^2} - AA_1}{2} + 22 \quad \text{(Eq. S1)}$$

We also plotted that the total displacement *u* distribution of the central *y*-*z* section of the heated region. It is found that the *u* is symmetrical with respect to the central position (see Fig. S6c).

S7. Influence of plasmonic heating on MSWA

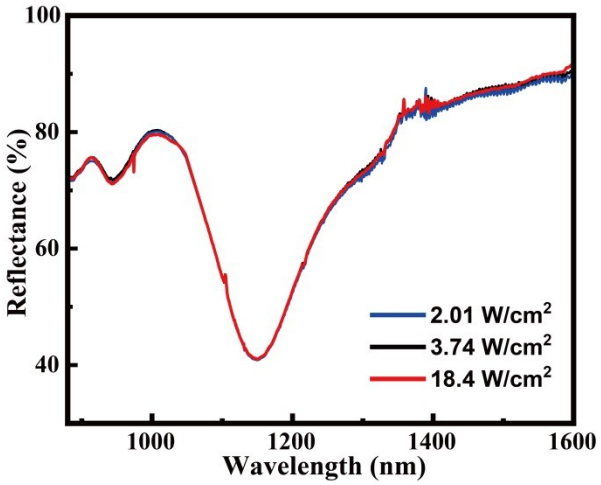

Fig. S7. Measured reflection spectra of a MSWA under incident light with different intensities at the resonant wavelength from 2.01 to 18.4 W/cm^2

S8. Absorption spectra of a MSWA on a PDMS slab

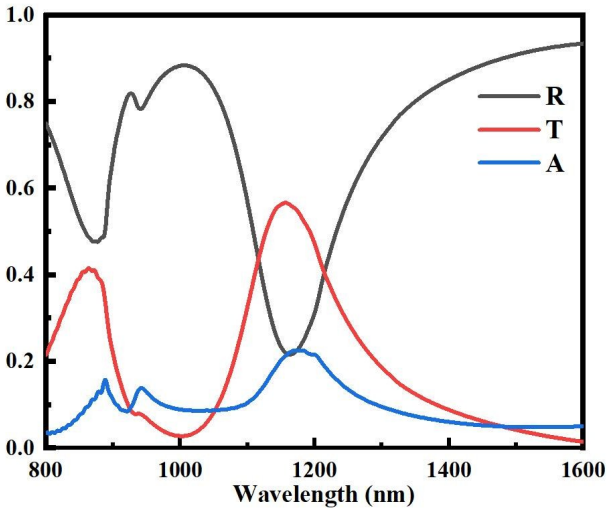

Fig.S8. Simulated reflection, transmission and absorption spectra of a MSWA on a PDMS slab.

S9. Calculation of the thermomechanical deformation of a MSWA on the PDMS substrate

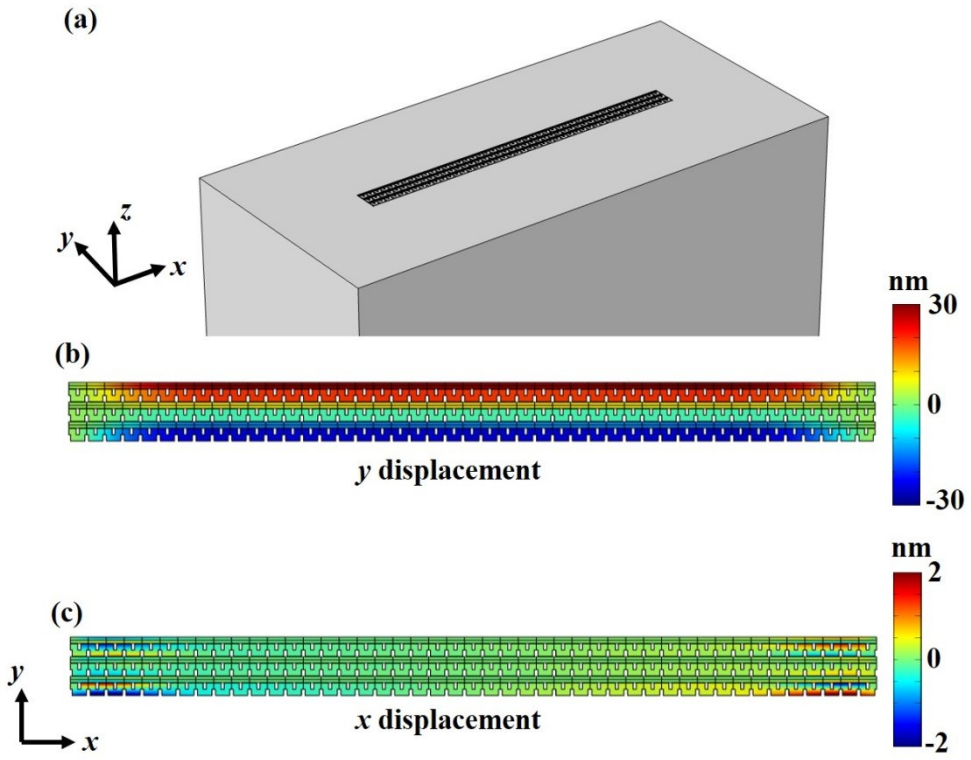

Fig. S9. (a) Modeling of a MSWA with 3 periods in *y*-axis and 45 periods in *x*-axis on the PDMS substrate. (b) Simulated displacement in *y*-axis distribution induced by applying a local temperature of 312.91 K. (c) Simulated displacement in *x*-axis distribution induced by applying a local temperature of 312.91 K.

S10. Calculation of temperature variation

To acquire the required thermal power for switching the PDMS substrate, a simple heat transfer model $I^2R = 2D\alpha\Delta T$ based on shape factors is provided here, where *I*, *R*, *D, α,* and ΔT stand for the injected current, resistance, array diameter, PDMS thermal conductivity and temperature variation, respectively. This model neglects convective heat transfer and assumes the system is in steady state. The resistor of the heating region is about 1.3 Ω and calculated by $R = \rho\frac{L}{S}$, where ρ is resistivity, L and S are the length and cross-sectional area of the gold nanostructures. Thus, the temperature variation ΔT with the different injected current can be calculated by the following equation:

$$\Delta T = 8.07 \times 10^4 \times I^2 \qquad \text{(Eq. S2)}$$

References

1 P. B. Johnson and R. W. Christy, *Phys. Rev. B* 1972, **6,** 4370-4379.

2 T. X. Chu, A. V. Salsac, E. Leclerc, D. Barthes-Biesel, H. Wurtz and F. Edwards-Levy, *J. Colloid Interf. Sci.* 2011, **355,** 81-88.

3 D. Qin, Y. Xia, and G. M. Whitesides, *Nat. Protoc.* 2010, **5,** 491-502.

4 J. E. Mark, *The polymer Data Handbook*, Oxford university press, 2009.

5 J. Y. Ou, E. Plum, L. Jiang and N. I. Zheludev, *Nano Lett.* 2011, **11,** 2142-2144.